UNIVERSITY OF BATH

Link to publication

University of Bath

A novel controller of a battery-supercapacitor hybrid energy storage system for domestic applications

Xudong Wang, Dongmin Yu, Simon Le Blond, Zhengming Zhao, Peter Wilson

Abstract—

Electrical energy storage is an attractive technology for complementing domestic scale Combined Heat and Power (CHP) because when CHP is dispatched to meet the heating load, the storage can reconcile any mismatch between the electrical load and CHP generation. Hybridization of electrical storage technologies reduces the compromise between power and energy density and extends storage system lifetime but necessitates a more complex control scheme. This paper proposes a novel control scheme for a domestic battery-supercapacitor hybrid energy storage system (HESS) for use with micro-combined heat and power (micro-CHP) generation. The proposed HESS controller utilizes the low frequency component of the supercapacitor voltage to generate the battery reference current, which not only allocates low frequency power to the battery but also simultaneously maintain the battery current and the supercapacitor voltage within their predefined limits. The negative effects of the 100 Hz ripple component in the supercapacitor current, such as overheating and increased converter losses have been hitherto neglected in the literature and are addressed here for the first time by adding a 100 Hz band-stop filter in the supercapacitor controller. Simulink simulations and signal hardware-in-the-loop (SHIL) real-time simulations have been conducted to demonstrate the effective operation of the HESS.

*Index Terms—***Hybrid Energy Storage Systems, Energy Storage, Hardware-in-the-loop, Simulation.**

1. Introduction

Domestic electricity is responsible for the most significant portion (approximately 30%) of total electricity demand in the UK [1]. Using distributed generation (DG) to provide energy to domestic buildings is seen as a promising way of reducing energy losses and carbon emissions. In addition to small localized wind turbines and photovoltaic systems, micro-combined heat and power (micro-CHP) shows promise at the domestic level for improving energy efficiency due to the cogeneration of heat and power [2]. One of the key issues, however, is the ability of the local distributed generation system to cope with wide variations in demand, and the limitations of the renewable energy sources to adapt to those variations.

Energy storage systems (ESS) have been widely investigated in power systems at various scales due to their inherent ability to load shift, which in particular makes ESS a potentially ideal solution for domestic demand response management [3]. Micro-CHP has a broadly constant ratio of power output to heat output whereas, in contrast, the ratio of power demand to heat demand in a domestic setting is highly variable. ESS is therefore an essential feature of buildings using micro-CHP by providing a buffer against this mismatch. A single technology ESS has limited characteristics in terms of cost, lifetime, power and energy density, depending on the energy storage technology it uses [4], therefore, hybrid energy storage systems (HESS) have been proposed to overcome these limits by harnessing the advantages of different energy storage technologies.

One widely proposed HESS is composed of a combination of batteries and supercapacitors, which have been used for electric vehicles (EV) [5], renewable energy systems (RES) [6] and domestic buildings [7]. The battery-supercapacitor HESS has the advantage of both high energy density and high power density and can therefore be used both for long term energy management by the batteries and fast

dynamic power regulation by the supercapacitors [6].

There are three main topologies of battery-supercapacitor HESS: passive, semi-active and active, which are shown in Fig. 1.
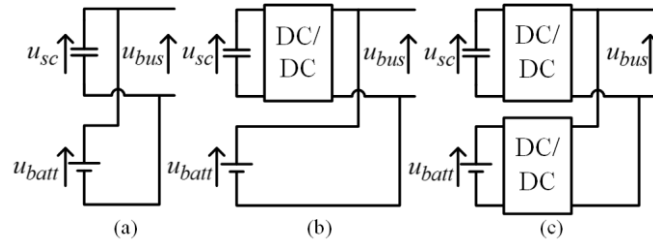

Fig. 1. Three main topologies of HESS: (a) Passive, (b) Semi-active, (c) Active.

The passive HESS is the simplest and lowest-cost topology, however the supercapacitor cannot be used effectively because the voltage of the supercapacitor must be equal to that of the battery and cannot be varied over a wide range [8].

The semi-active topology adds a power electronic converter between the supercapacitor and the DC bus, while the battery is directly connected to the DC bus. This topology decouples the supercapacitor and the battery, but the current of the battery cannot be conditioned directly, which may have a negative effect on the lifetime of the battery [9].

The active HESS uses dedicated converters for the supercapacitor and the battery, and is the most commonly used configuration. The advantage of this configuration is that both the current from the battery and the current from the supercapacitor can be controlled actively [10]. Given the highest level of flexibility it offers, the active HESS is adopted in this paper for the optimal control of both the supercapacitor and the battery.

Currently, various control strategies have been proposed for HESS, such as dynamic programming (DP) [11], model predictive control (MPC) [12, 13], fuzzy logic control (FLC) [14], rule-based control (RBC) [15, 16], and filter-based control (FBC) [17, 18].

A DP method can be used to optimize energy management of HESS by searching the optimum operational point at each time step [11]. However, as described in [11], the optimization only focuses on the lifetime of the battery and the operation is not comprehensively evaluated. The MPC method, which has been verified by simulation [12] and experiment [13], relies on accurate modeling of the system and a cost function for prediction and control. However, there can be significant computational demand, especially if higher order models of batteries and supercapacitors are used [17]. The FLC method proposed in [14] is used for energy management for a hybrid supercapacitor/battery/fuel cell system. However, it also requires the wavelet transform to split the power demand, which adds to the complexity of the controller. The RBC method has also been used for energy management of HESS in wireless sensors [15] and electric vehicles [16]. However, the rules are mainly determined by experience and expert knowledge, and are subject to the specific application.

The FBC method used in [17] and [18] allocates the high frequency component of power demand to the supercapacitor and the low frequency component to the battery by a filter, which is straightforward and easy to implement. In [17], a low complexity FBC method is proposed to maintain operation within the system's important operational limits, however, the considerations of the application side are not addressed. In [18], the FBC method is implemented to control the grid-connected HESS and the 100 Hz current ripple is allocated to the supercapacitor. Although in [18], the 100 Hz ripple component in the supercapacitor current waveforms is filtered out to highlight its response to fast power changes, the negative effects of the 100 Hz ripple are significant. On one hand, as the time constant of the

supercapacitor is much higher than that of an electrolytic capacitor, exposing supercapacitors to a continuous ripple current may cause overheating [19]. On the other hand, the 100 Hz ripple will be amplified corresponding to the lower voltage of the supercapacitor compared to the DC bus, resulting in more power loss within the converter.

Another important aspect in the controller design is the monitoring and protection of the HESS states, such as supercapacitor voltage, battery current and battery SOC. Commonly, the states of the supercapacitor and the battery are maintained independently, which however, can restrict the utilization of the HESS in some cases when only the supercapacitor or the battery reaches its safe limit. Therefore, a coordinated control that considers all HESS states simultaneously is desirable to maximize overall system utilization.

The main contributions of this paper are: 1) a novel controller is proposed, which harnesses the low frequency component of the supercapacitor voltage to both allocate low frequency power to the battery and also simultaneously maintain the supercapacitor voltage and the battery current within their limits; 2) the 100 Hz ripple current is allocated to the DC bus capacitor instead of the supercapacitor side to protect the supercapacitor and reduce losses in the converter; 3) the control strategy is verified through MATLAB simulation and signal hardware-in-the-loop (SHIL) testing considering time-of-use tariffs and load fluctuations. The SHIL plays an important role in verification as an intermediary step before implementation in an actual real world system due to the following advantages [20,21]:

1) By connecting the controller hardware in a closed loop with real time simulation tools such as the Real Time Digital Simulator (RTDS), the controller can be tested in a realistic hardware implementation, for example as a Digital Signal Processor (DSP) that processes real time analogue signals.

2) By using the small time step capability of the real time simulator (in this case, sub 2.5 μs) simulation accuracy required for power conversion is maintained without sacrificing the real time requirement.

3) The control system can be verified under both normal dynamic operation, and fault and other transient conditions easily and inexpensively, reducing the need for expensive real world testing.

This paper is organized as follows. In section 2, the whole system is described in terms of the circuit topology, the system parameters and the modeling of the supercapacitor, the battery and the CHP generation. Section 3 presents the control strategy for the HESS, including system operational strategies and detailed control methods for the converters. In section 4, electromagnetic transient phenomena of the controller, such as the current ripple of the supercapacitor and the voltage fluctuation of the DC bus are studied with SIMULINK. The SHIL real-time verification of the system operation is presented in section 5, with the conclusions given in section 6.

2. System configuration and modeling

2.1 System configuration

Fig. 2 shows the electrical diagram of a typical domestic energy system with CHP (combined heat and power) and hybrid energy storage systems (HESS). Two bidirectional buck-boost converters are used to connect the supercapacitor and battery to the local DC bus, which is then connected to the grid with an H-bridge DC/AC converter. The CHP, which is regarded as a promising technology for increasing overall domestic energy efficiency, is also included in this system. However, since the focus is on electric energy management, the heat generation from the CHP is not considered in this paper. Table I lists the system parameters.
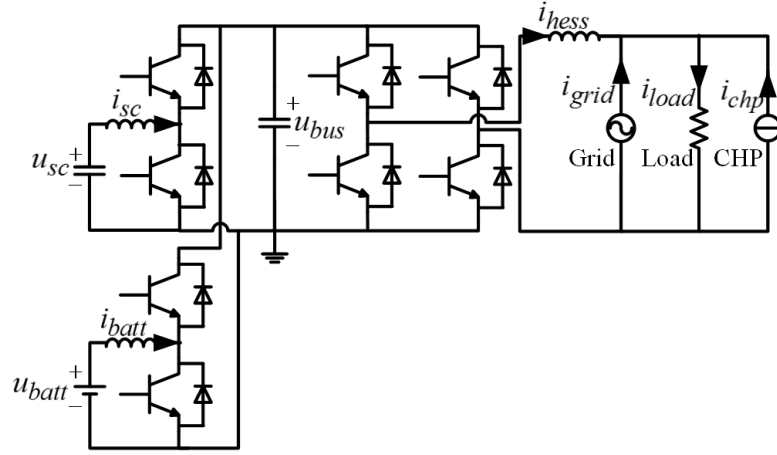
Fig.2 Electrical diagram of a domestic energy system with CHP and HESS.

Table I. System parameters

C_{sc}	144 F	R_{esr}	2.1 mΩ	$u_{sc(nom)}$	24 V	$u_{bus(nom)}$	500 V
Q_{batt}	720 Ah	$u_{batt(nom)}$	24 V	$p_{load(max)}$	3000 W	$u_{grid(nom)}$	230 V
$i_{batt(max)}$	125 A	$i_{batt(min)}$	−125 A	$i_{sc(max)}$	300 A	$i_{sc(min)}$	−300 A
L_{sc}	0.1 mH	L_{batt}	5 mH	L_{grid}	20 mH	p_{chp}	600 W

2.2 System Modeling

A. Modeling of supercapacitor

The supercapacitor model used in this paper is a simple serial RC model. This model provides simplicity and sufficient accuracy, and has been used for validating HESS in electric vehicles [5] and residential energy systems [20].

B. Modeling of battery

The battery type chosen in this work is the lead-acid battery, which is suitable for domestic applications due to its technical maturity and relative low cost [22]. The battery model is a controlled voltage source with a series resistor, shown in Fig. 3 [23]. In [23], the model has been validated using discharge curves of a 12 V/1.2 Ah Lead-Acid battery. Some model parameters are listed in Table II.
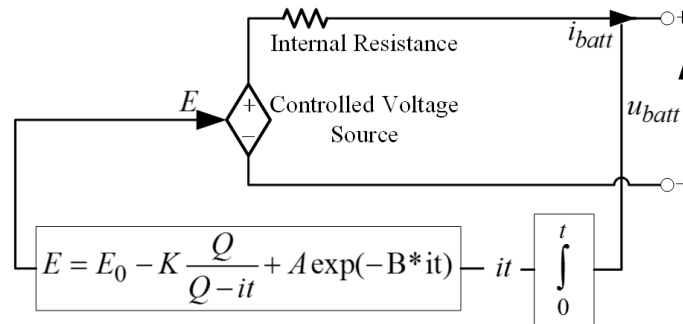

$$E = E_0 - K \frac{Q}{Q-it} + A \exp(-B*it) - it$$

Fig. 3. Battery Model [23].

TABLE II. Battery Model Parameters

$E_0(V)$	12.6463	$A(V)$	0.66
$R(\Omega)$	0.25	$B(Ah^{-1})$	2884.61
$K(V)$	0.33	$Q(Ah)$	1.2

C. Modeling of micro-CHP

A complete system schematic and model of micro-CHP has been proposed in [24], which however is more complex than is required for this work. Since the focus is on studying the optimal electric power split strategy of the HESS, only the electric output of the CHP needs to be considered. Therefore, this paper uses a current source to model the electric output of CHP. Although the output can be variable due to different control strategies applied to the micro-CHP, a constant output current is assumed in this paper for simplicity, and the influence of variable output of the micro-CHP on the performance of HESS can be represented by using variable load profile.

2.3 Cost analysis

The cost of the HESS system is mainly subjected to the sizing of both energy storage systems. The estimated energy price of battery and supercapacitor in [25] is used for the cost analysis. According to the HESS sizing shown in Table I, the cost of the 3.0 kW HESS system is shown in Table III.

TABLE III. Cost analysis of the HESS system

	Size	Energy price	Cost
Battery	17.28 kWh	3000 $/kWh	51,840 $
Supercapacitor	0.012 kWh	10000 $/kWh	120 $

In this example case, the cost of the supercapacitor accounts for only 0.23% of the total cost of the HESS system. It should be noted that a more detailed cost analysis is required to optimize the sizing of the HESS system, which is not the scope of this paper and will be addressed in future work. Still, the small cost portion of the supercapacitor can be expected in domestic applications with lower level of power fluctuations than most industrial applications.

3.   Control strategy

The proposed HESS controller is composed of the battery and supercapacitor controller circuits. The AC side control is also introduced in this section with a power demand controller to generate power demand for the HESS and a controller of the AC/DC converter.

3.1 Battery controller

Fig. 4 (a) shows the structure of the battery controller. The power sharing strategy implemented in the current generator module is shown in Fig. 4 (b).
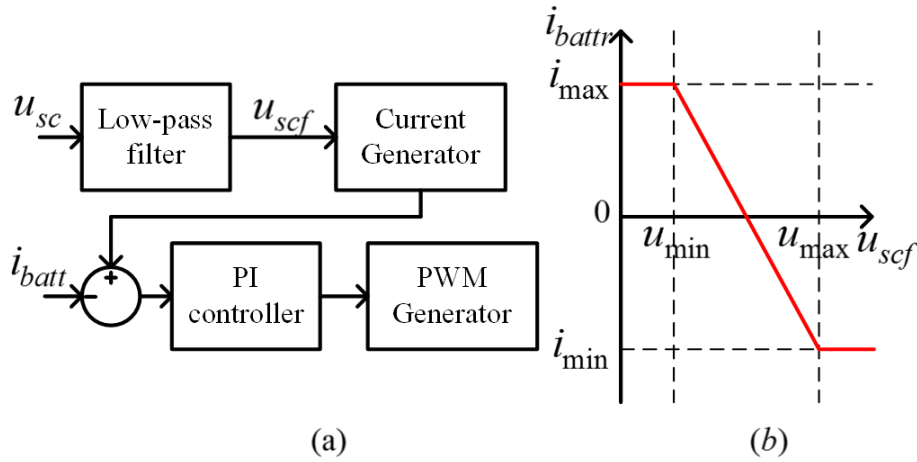

Fig. 4. Battery controller. (a) The structure of battery controller, (b) the power sharing strategy.

In the power sharing strategy, i_{battr} is the battery reference current, which is generated according

to u_{scf}, the low frequency component of u_{sc}. Here, u_{scf} is used to filter out the high frequency ripple caused by the ESR of the supercapacitor, therefore the transfer function of the low-pass filter is (1):

$$F_{lp}(s) = \frac{1}{1+sC_{sc}R_{esr}}$$ (1)

where $R_{esr} = 2.1\ m\Omega$ is the equivalent series resistance of the supercapacitor. Therefore, the power sharing strategy in which the battery reference current i_{battr} is a linear function of u_{scf}, presents a low-pass feature, with the cut-off frequency given in (2):

$$f_c = \frac{1}{2\pi C_{sc}R_{esr}} = \frac{1}{2\pi \times 144F \times 2.1m\Omega} \approx 0.5Hz$$ (2)

Compared with the commonly used FBC method, where the total required current is allocated to the supercapacitor and the battery by a high-pass or low-pass filter, the proposed strategy can not only split the power demand based on the low frequency component of the supercapacitor voltage, but also provide a coordinated control between the battery and the supercapacitor by considering the limits of u_{sc} and i_{batt} simultaneously. The limits of i_{batt} are listed before in Table I. For the voltage range of the supercapacitor, $u_{sc\,max}$ is the nominal voltage $u_{sc\,nom}$, and $u_{sc\,min}$ is set to be $1/2\,u_{sc\,nom}$, to allow 75% of the energy of the supercapacitor to be used. It should be noted that the cut-off frequency in (2) is related to C_{sc}. In some cases, when the required capacity of the supercapacitor is too small, the low-pass filter must to be adjusted as (3):

$$F_{lp}(s) = \frac{1}{1+skC_{sc}R_{esr}}$$ (3)

where k is a constant to generate suitable cut-off frequency for the battery current.

3.2 Supercapacitor controller

The function of the supercapacitor controller is to keep u_{bus} stable. Thus, the whole power demand is supplied by the HESS, given by (4):

$$p_{sc} + p_{batt} = p_{demand}$$ (4)

As presented in section 3.1, the battery is only responsible for the low frequency power demand, so the high frequency power fluctuation is allocated to the supercapacitor.

The supercapacitor controller as shown in Fig. 5, is a double loop controller. The outer loop tracks u_{bus} to keep it stable, and the inner loop regulates the supercapacitor current. By adding a 100 Hz band-stop filter, the 100 Hz component of the reference current is filtered out. So the 100 Hz power fluctuation is transferred from the low-voltage supercapacitor side to the high-voltage DC bus side, beneficial for the thermal protection of the supercapacitor and lower losses in the DC-DC converter. The transfer function of the filter is shown in (5):

$$H(s) = \frac{s^2+395000}{s^2+888s+395000}$$ (5)

The Bode plot is shown in Fig. 6. A feed-forward control is added to improve the dynamic response of the controller. Based on (4), the feed-forward current is calculated by (6):

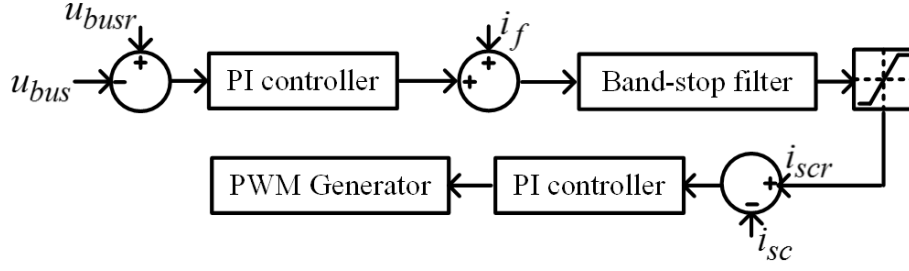$$i_f = (p_{demand} - i_{batt} \times u_{batt})/u_{sc}$$ (6)

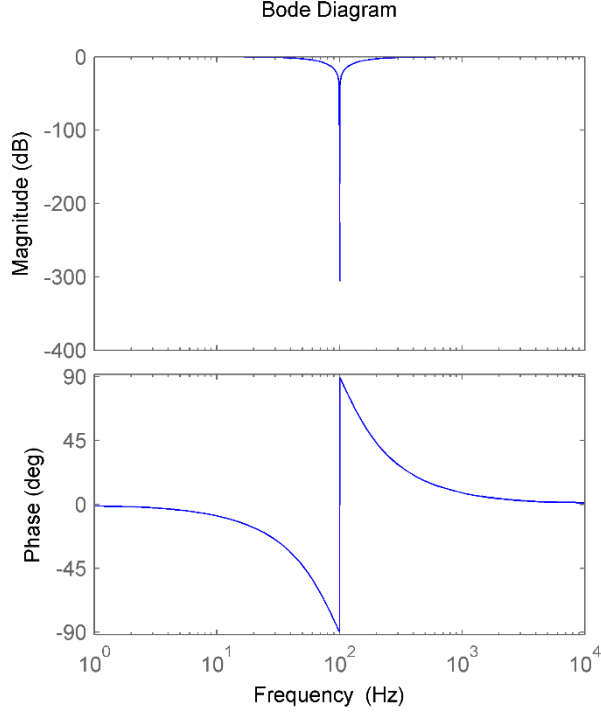Fig. 5. Supercapacitor controller.

Fig. 6. Bode plot of the 100 Hz Band-stop filter.

3.3 AC side control

A. Power demand controller

The main function of the power demand controller is to generate the power demand for the HESS based on load profiles, HESS state, time-of-use electric tariffs and the battery SOC. Fig. 7 shows the operational strategy. The *HESS State* block judges if the HESS should discharge or charge according to the power difference p_{diff} between the load and the CHP, with the criterion given in (7):

$$state = \begin{cases} 1 & if\ p_{diff} > 0\ (for\ discharge) \\ 0 & if\ p_{diff} \leq 0\ (for\ charge) \end{cases} \tag{7}$$

The *SOC Monitor* block monitors the SOC of the battery by given flag signals $flag_{soc+}$ and $flag_{soc-}$ to indicate whether the SOC has reached the maximum value and minimum value respectively. The values of $flag_{soc+}$ and $flag_{soc-}$ are defined in (8) and (9).

$$flag_{soc+} = \begin{cases} 1 & if\ SOC \geq SOC_{max} \\ 0 & if\ SOC < SOC_{max} \end{cases} \tag{8}$$

$$flag_{soc-} = \begin{cases} 1 & if\ SOC \leq SOC_{min} \\ 0 & if\ SOC > SOC_{min} \end{cases} \tag{9}$$

The conforming energy price in [3] is used in this paper. In the conforming case, the variation trend

of energy price follows the variation of demand. And the selling and purchasing prices are assumed the same. The *Tariff Info* block stores the tariff information and judges whether the current tariff is high ($tariff = 1$) or low ($tariff = 0$). (Here, two tariff states are used for simplicity, although more tariff states and the energy management strategies based on these states can be defined through a straightforward process.) An enable signal is then generated by considering the HESS state, the tariff information and the SOC of the battery, with the logic operations shown in Fig. 7.

The time series in Fig. 8 shows two examples of how power varies when this strategy is deployed. During high tariff period, when p_{load} is higher than p_{chp}, the HESS will discharge to meet the power demand. When p_{load} is lower than p_{chp}, however, the surplus power generated by micro-CHP will be sold to the grid. This will thus yield maximum benefits to householders by exchanging the roles of the HESS and the grid. Likewise, during the low tariff period, it is preferable to purchase power from the grid at higher load power and charge the HESS at lower load power, so the surplus power can be stored in the HESS for use during the high tariff period. When the HESS is disabled due to the battery reaching its SOC limits, the power difference will be supplied by the grid. It should be noted that in real applications, the output power of m-CHP can be estimated by the control schemes and the residential load power can be estimated by real-time measurements or residential load forecasting. Then with these information, the surplus power generated by micro-CHP or the power difference p_{diff} can be calculated, as shown in Fig. 7.
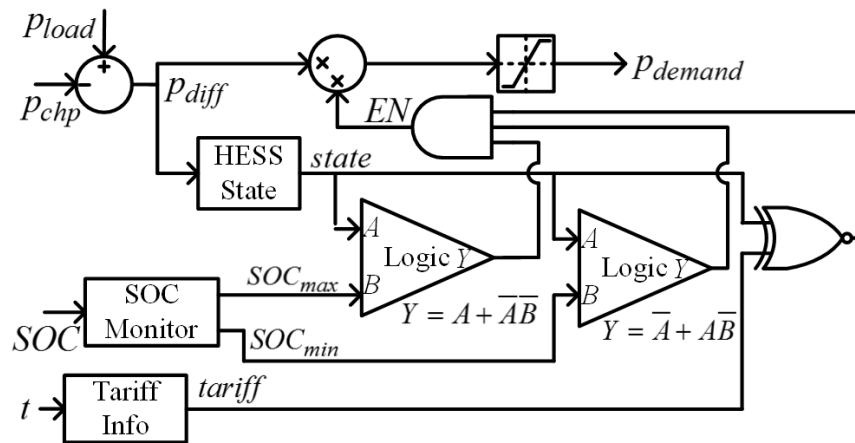

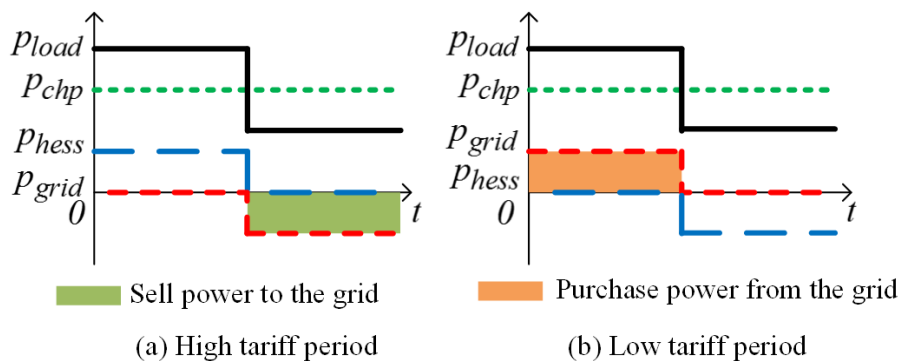Fig. 7. Operational strategy of the power demand generator

(a) High tariff period   (b) Low tariff period

Fig. 8. Example case during (a) high tariff period and (b) low tariff period.

B. Controller of the AC/DC converter

The AC/DC converter transfers the required power between the HESS and the grid. The control strategy is shown in Fig. 9. To regulate the output current of the HESS, the reference current is generated

by (10),

$$i_{demand} = (i_{load} - i_{chp}) \times EN \qquad (10)$$

where EN is the enable signal generated in the power demand generator, which is then also used to control the PWM output as an enable signal.
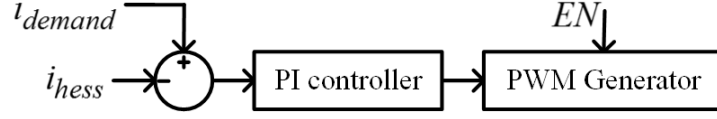

Fig. 9. Controller of the AC/DC converter.

4. SIMULINK validation

A system simulation based on Fig. 2 was built using MATLAB SIMULINK, to analyze the transient responses of the HESS including the proposed controllers during various load power fluctuation scenarios.

The switching frequencies of all three power electronic converters were set to be 10 kHz, with a simulation step of 1 μs. The PI parameters for the controllers are listed in Table IV.

Table IV. PI Parameters

Controller	Proportional Gain	Integral Gain
Battery controller	10	100
Supercapacitor inner loop	1	10
Supercapacitor outer loop	4	10
AC-DC converter	10	100

An example case under high tariff conditions shown in Fig. 8(a) was simulated where the load power changes from 2000 W to 400 W at t = 12 s. In Fig. 10, the currents of $i_{chp}, i_{batt}, i_{grid}$ and i_{hess} are shown at the load power changing point. The supplier of the power demand changes from the HESS to the grid, which shows the effectiveness of the power demand controller. Fig. 11 illustrates the DC bus voltage and the current and voltage waveforms of the HESS. At t = 12 s, the battery current shows a slow variation due to its duty of meeting the low frequency power demand, while the supercapacitor current shows a fast current variation to absorb the power output from the battery when the power demand is transferred from the HESS to the grid. The supercapacitor current overshoot at t = 12 s results from the logic delay of the enable signal EN after the power changes. Thus, the power demand will first go down to a negative value then back to zero, which further influences the value of the feed-forward current to the supercapacitor controller. Considering this very short delay (less than 10 μs in MATLAB simulation) and the current limiter in the supercapacitor controller, the current overshoot problem is negligible.

Fig. 12 compares the supercapacitor current waveforms with and without the 100 Hz band stop filter in the controller, which shows that before t=12 s, when the HESS is discharging, the 100 Hz ripple current on the supercapacitor side is significantly reduced by adding the band-stop filter. The ripple current will cause surplus losses in the supercapacitor and the converter. The power losses in two cases are compared in (11),

$$\frac{p_{case1}}{p_{case2}} = \frac{(I_{dc}^2 + I_{ripple}^2)R_{es}}{I_{dc}^2 R_{es}} = 20.7 \qquad (11)$$

where p_{case1} and p_{case2} represent the power losses (11.5s<t<12s) in the two cases shown in Fig. 12,

and R_{es} represent the equivalent series resistance. As shown in (11), by adding the band-stop filter, significant loss reduction on the supercapacitor side is found. After t=12 s, there is only DC power transferring from the battery to the supercapacitor, therefore there are on 100 Hz ripples in both cases.

The HESS also works as a back-up power supply in case of the power failure, when the HESS will supply the domestic load with the micro-CHP. The back-up time t_b is given in (12).

$$t_b = \frac{(SOC_{ini} - SOC_{min})Q_{batt}u_{batt(nom)}}{p_{load} - p_{chp}} \tag{12}$$

Assuming $SOC_{ini} = 100\%$ and $SOC_{min} = 50\%$, when p_{load} reaches the maximum load power 3.0 kW, the back-up time t_b is 3.6 h, based on (12).
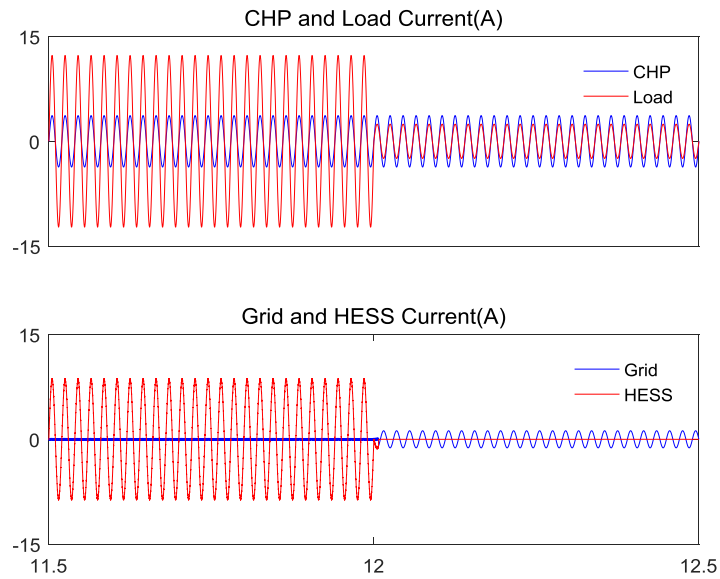

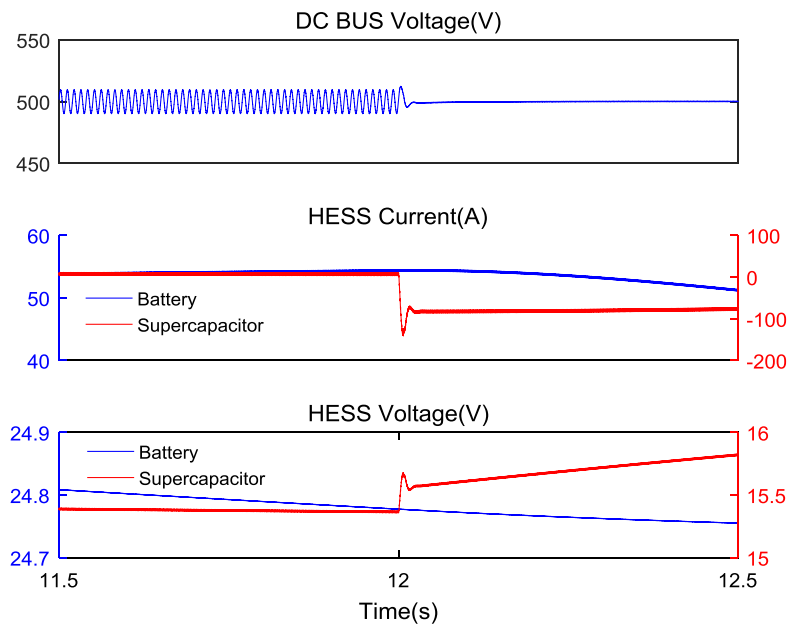Fig. 10. Simulation results of currents at the power changing point.

Fig. 11. Simulation results of the HESS operation at the power changing point.
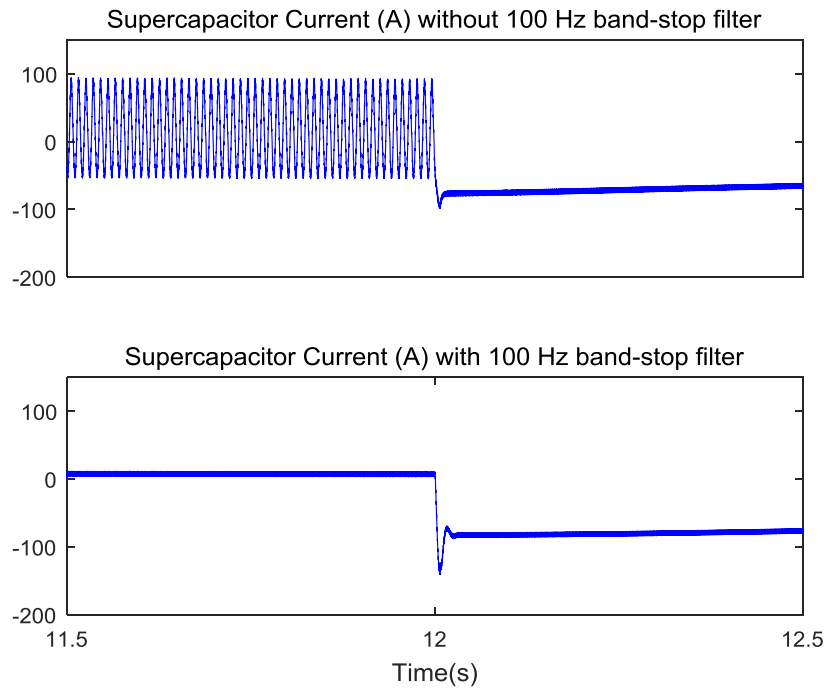
Fig. 12. Simulation results of the supercapacitor current with and without 100 Hz band-stop filter.

5. Real-time Verification using SHIL

In order to verify the controller of the HESS, some real-time SHIL results are analyzed, which offers the same environment in the real world from the controller side. Fig. 13 shows the SHIL configuration for the real-time verification of the HESS controller. The primary system and the power demand controller were simulated on an RTDS system [26]. The main time-step in RTDS is $50\ \mu s$, while the power electronics converters are built in the VSC sub-network, with a time-step of $2.08\ \mu s$. The HESS controller was implemented in real time code running on a customizable DSP board, which captures the analogue output signals from the ODAC card in the RTDS [26]. The PWM pulses generated by the DSP are read by the RTDS through its GTDI card, which samples every 320 ns [27].
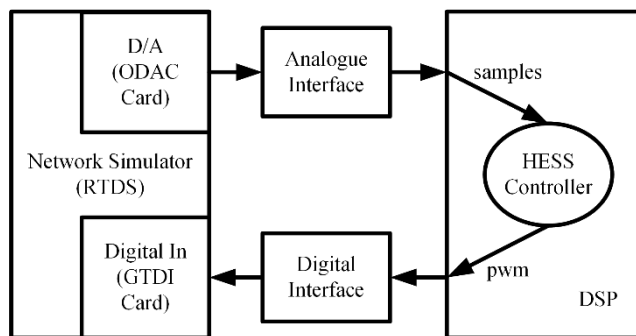

Fig. 13. The system HIL configuration.

Since the sampling rate of the ODAC card is $50\ \mu s$, the switching frequencies of the DC/DC converters for the battery and the supercapacitor were reduced to 2.5 kHz and 5 kHz respectively to increase the resolution of the duty cycles for the PWM pulses with the results shown in Fig. 14 and Fig. 15.

Fig. 14 shows the HESS operation in the high tariff period (left) and the low tariff period (right). Here, the power demand means the power difference between the load power and the output

electric power from CHP. In the high tariff period, the HESS discharges when the power demand is above zero ($p_{load} > p_{CHP}$), and no power is supplied from the grid. However, when the power demand is below zero ($p_{load} < p_{CHP}$), the power demand is entirely supplied from the grid, and the power output from the HESS is held at zero. The roles of the grid and the HESS are reversed in the low tariff period, verified in Fig. 14, which also shows how the supercapacitor responds to the high frequency power demand variation, while the battery fills the low frequency power demand.

Fig. 15 shows the HESS operation when the SOC hits the maximum and minimum limits, set at 80% and 50% respectively in these example cases. In both cases, the power output of the HESS is set to zero when the SOC hits its limit, and the power demand is then supplied by the grid. The control system therefore protects the battery by maintaining its SOC within these predefined limits.
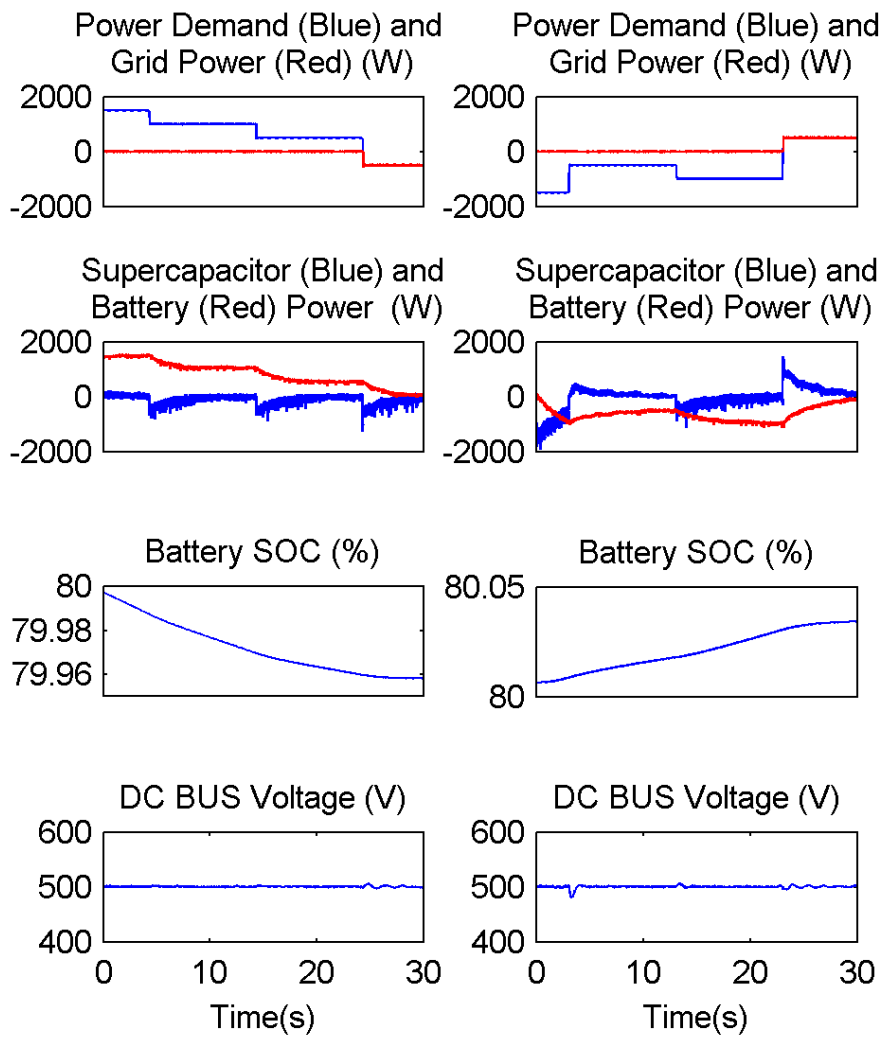

Fig. 14. Real-Time SHIL simulation results (Left: High Tariff Period, Right: Low Tariff Period). (Data sampling interval: 0.0004 s).
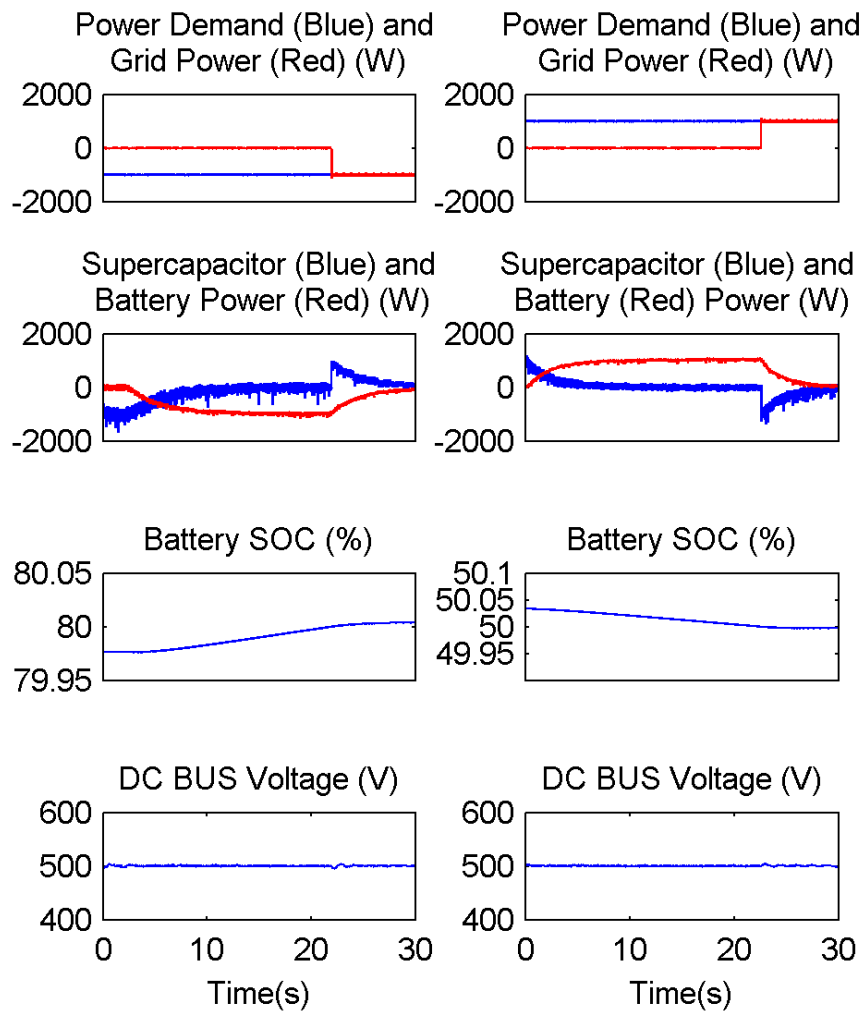
Fig. 15. Real-Time SHIL simulation results (Left: Maximum SOC, Right: Minimum SOC). (Data sampling interval: 0.0004 s).

6. Conclusions

In this paper, a novel controller for a battery-supercapacitor HESS is proposed and verified in both SIMULINK simulation and SHIL real-time simulation. The SIMULINK simulation verifies the coordinated operation of the supercapacitor and the battery at the power changing point, and demonstrates that the proposed controller can effectively reduce the 100 Hz current ripple in the supercapacitor current, which otherwise can cause the supercapacitor to overheat and increase losses in the converter. The SHIL real-time simulation is an important next step to verify the HESS controller in a real-time environment by virtue of processing real physical signals, and implementation of the control algorithm using real hardware. The SHIL simulation results show that the supercapacitor responds to rapid power changes while the battery responds to slow power changes. Also, the control scheme coordinates power flow effectively between the HESS and the grid, making use of tariff periods and HESS states to maximize the benefits to householders and maintain the HESS within safe operational limits. The main advantages of the proposed controller are the coordinated control which simultaneously maintains the supercapacitor voltage and the battery current within safe limits and the effective attenuation of the 100 Hz current ripple on the supercapacitor side resulting in lower losses and thermal protection of the supercapacitor.

References:

[1] National Statistics (2015, July), "Electricity: Chapter 5, Digest of United Kingdom Energy Statistics (DUKES)," [Online]. Available: https://www.gov.uk/government/statistics/electricity-chapter-5-digest-of-united-kingdom-energy-statistics-dukes.

[2] M. Houwing, R. R. Negenborn and B. De Schutter, "Demand Response With Micro-CHP Systems," *Proceedings of the IEEE,* vol. 99, pp. 200-213, 2011.

[3] Z. Wang, C. Gu, F. Li, P. Bale, and H. Sun, "Active Demand Response Using Shared Energy Storage for Household Energy Management," *IEEE Transactions on Smart Grid,* vol. 4, pp. 1888-1897, 2013.

[4] Y. Kim, J. Koh, Q. Xie, Y. Wang, N. Chang, and M. Pedram, "A scalable and flexible hybrid energy storage system design and implementation," *Journal of Power Sources,* vol. 255, pp. 410-422, 2014.

[5] Z. Song, H. Hofmann, J. Li, X. Han, and M. Ouyang, "Optimization for a hybrid energy storage system in electric vehicles using dynamic programing approach," *Applied Energy,* vol. 139, pp. 151-162, 2015.

[6] T. Ma, H. Yang and L. Lu, "Development of hybrid battery – supercapacitor energy storage for remote area renewable energy systems," *Applied Energy,* vol. 153, pp. 56-62, 2015.

[7] X. P. Chen, Y. D. Wang, H. D. Yu, D. W. Wu, Y. Li, and A. P. Roskilly, "A domestic CHP system with hybrid electrical energy storage," *Energy and Buildings,* vol. 55, pp. 361-368, 2012.

[8] Z. Song, H. Hofmann, J. Li, X. Han, X. Zhang, and M. Ouyang, "A comparison study of different semi-active hybrid energy storage system topologies for electric vehicles," *Journal of Power Sources,* vol. 274, pp. 400-411, 2015.

[9] S. Vazquez, S. M. Lukic, E. Galvan, L. G. Franquelo, and J. M. Carrasco, "Energy Storage Systems for Transport and Grid Applications," *IEEE Transactions on Industrial Electronics,* vol. 57, pp. 3881-3895, 2010.

[10] H. Jung, H. Wang and T. Hu, "Control design for robust tracking and smooth transition in power systems with battery/supercapacitor hybrid energy storage devices," *Journal of Power Sources,* vol. 267, pp. 566-575, 2014.

[11] M. Masih-Tehrani, M. Ha'Iri-Yazdi, V. Esfahanian, and A. Safaei, "Optimum sizing and optimum energy management of a hybrid energy storage system for lithium battery life improvement," *Journal of Power Sources,* vol. 244, pp. 2-10, 2013.

[12] A. Santucci, A. Sorniotti and C. Lekakou, "Power split strategies for hybrid energy storage systems for vehicular applications," *Journal of Power Sources,* vol. 258, pp. 395-407, 2014.

[13] B. Hredzak, V. G. Agelidis and M. Jang, "A model predictive control system for a hybrid battery-ultracapacitor power source," *Power Electronics, IEEE Transactions on,* vol. 29, pp. 1469-1479, 2014-01-01 2014.

[14] O. Erdinc, B. Vural and M. Uzunoglu, "A wavelet-fuzzy logic based energy management strategy for a fuel cell/battery/ultra-capacitor hybrid vehicular power system," *Journal of Power Sources,* vol. 194, pp. 369-380, 2009.

[15] F. Ongaro, S. Saggini and P. Mattavelli, "Li-Ion Battery-Supercapacitor Hybrid Storage System for a Long Lifetime, Photovoltaic-Based Wireless Sensor Network," *IEEE Transactions on Power Electronics,* vol. 27, pp. 3944-3952, 2012.

[16] J. P. Trovão, P. G. Pereirinha, H. M. Jorge, and C. H. Antunes, "A multi-level energy management system for multi-source electric vehicles – An integrated rule-based meta-heuristic approach," *Applied Energy,* vol. 105, pp. 304-318, 2013.

[17] B. Hredzak, V. G. Agelidis and G. D. Demetriades, "A low complexity control system for a hybrid DC power source based on ultracapacitor–lead–acid battery configuration," *Power Electronics, IEEE Transactions on,* vol. 29, pp. 2882-2891, 2014-01-01 2014.

[18] D. B. W. Abeywardana, B. Hredzak and V. G. Agelidis, "Single-Phase Grid-Connected LiFePO4 Battery-Supercapacitor Hybrid Energy Storage System With Interleaved Boost Inverter," *Power Electronics, IEEE Transactions on,* vol. 30, pp. 5591-5604, 2015-01-01 2015.

[19] Maxwell Technologies (2015), "Design Considerations For Ultracapacitors," [Online]. Available: http://www.maxwell.com/images/documents/technote_designinguide.pdf.

[20] W. Li, G. Joós and J. Bélanger, "Real-time simulation of a wind turbine generator coupled with a battery supercapacitor energy storage system," *Industrial Electronics, IEEE Transactions on,* vol. 57, pp. 1137-1145, 2010-01-01 2010.

[21] Li J, Wang X, Zhang Z, et al. "Analysis of a new design of the hybrid energy storage system used in the residential m-CHP systems." *Applied Energy,* vol. 187, pp.169-179, 2017.

[22] M. Dürr, A. Cruden, S. Gair, and J. R. McDonald, "Dynamic model of a lead acid battery for use in a domestic fuel cell system," *Journal of Power Sources,* vol. 161, pp. 1400-1411, 2006.

[23] O. Tremblay, L. Dessaint and A. Dekkiche, "A generic battery model for the dynamic simulation of hybrid electric vehicles," *Vehicle power and propulsion conference*, *IEEE*, pp. 284-289, 2007.

[24] A. Arsalis, M. P. Nielsen and S. K. Kær, "Modeling and parametric study of a 1kWe HT-PEMFC-based residential micro-CHP system," *International Journal of Hydrogen Energy,* vol. 36, pp. 5010-5020, 2011.

[25] Guo, Feng, and Ratnesh Sharma. "Hybrid Energy Storage Systems integrating battery and Ultracapacitor for the PJM frequency regulation market." Power and Energy Society General Meeting (PESGM), 2016. IEEE, 2016.

[26] RTDS Technologies, "Power System Users' Manual," December, 2012.

[27] RTDS Technologies, "Hardware Manual," January, 2009.